Electronic Supplementary Information (ESI) for Chemical Communications

Single-layer CoFe hydroxides for efficient electrocatalytic oxygen evolution

Yi Zhou,[#,a] Jialai Hu,[#,a], Dan Li,[a] and Qingsheng Gao*

College of Chemistry and Materials Science, and Guangdong Provincial Key Laboratory of Functional Supramolecular Coordination Materials and Applications, Jinan University

Guangzhou 510632, P. R. China

E-mail: tqsgao@jnu.edu.cn

[#]These authors contribute equally to this work.

Experimental section

Synthesis of single-layer CoFe LDH (CoFe LDH-*S*) nanosheets

The synthesis of CoFe LDH-*S* nanosheets followed a novel co-precipitation strategy. In short, 0.6 mmol $CoCl_2 \cdot 6H_2O$ and 0.4 mmol $Fe(NO_3)_3 \cdot 9H_2O$ (98.5%, Shanghai Macklin Biochemical) were dissolved in 40 mL of absolute EtOH (AR, Guangzhou Chemical Reagent Factory). Afterwards, 5 mmol of sodium bicarbonate (NH_4HCO_3, 99.995%, Shanghai Aladdin Biochemical Technology) was added into the precursor solution under vigorous stirring for 8 h. Thereafter, as-obtained precipitants were collected by centrifugation before washed by three times with water and ethanol, and CoFe LDH-*S* was subsequently dried in an oven at 60 °C overnight.

The preparation of bulk CoFe LDH materials (CoFe LDH-*Bulk*) followed a co-precipitation and subsequent hydrothermal method reported elsewhere with minor modification.[1] In brief, 0.6 mmol $CoCl_2 \cdot 6H_2O$ and 0.4 mmol $Fe(NO_3)_3 \cdot 9H_2O$ were dissolved in 15 mL ultrapure water, and the alkaline mixed solution (15 mL) containing 1.6 mmol NaOH and 0.8 mmol Na_2CO_3 was also prepared in another separate beaker. Afterwards, the two separate aqueous solutions were simultaneously

added to a beaker under vigorous stirring for 10 min. The obtained slurry was then added into a stainless-steel Teflon-lined autoclave, and heated in an oven at 80 °C for 12 h. Then the precipitants were collected by centrifugation before washed by three times with water and ethanol, and CoFe LDH-*Bulk* was subsequently dried in an oven at 60 °C overnight.

Electrochemical measurements

The electrochemical tests were conducted with a typical three-electrode configuration on a CHI 760 electrochemical workstation. The mercuric oxide electrode (Hg/HgO) was used as reference electrode and the counter electrode was a graphite rod. Glassy carbon electrode, commercial Ni foam and carbon cloth were both used as working electrode for different purpose.

1) Glassy carbon electrode (GCE)

As for working electrode preparation, 4 mg of catalyst, 1 mg of acetylene black and 20 μL of Nafion solution were dispersed in ethanol (0.25 ml) and H_2O (0.75 ml) mixed solution under ultrasonication for 1 h to obtain a homogeneous catalyst ink. Afterwards, 5 μL of as-prepared ink was drop-cast onto a GCE with a diameter of 3 mm. If not specified, cyclic voltammetric (CV) scans were recorded at a scan rate of 5 mV s^{-1}. The electrochemical impedance spectroscopy (EIS) data were collected at 1.5 V vs. RHE using a 5 mV amplitude perturbation between 10 kHz and 0.1 Hz. The potential window of CV scans was 1.05 to 1.15 V vs. RHE for C_{dl} measurements, and the scan rates of CV scans were 20, 40, 60, 80, 100 and 120 mV s^{-1}, respectively.

2) Commercial Ni foam

To avoid the "bubble overpotentials" on a flat GCE and the resultant detachment of catalyst from the electrode as O_2 evolves,[2, 3] the extended duration of OER stability was inquired by using porous Ni foam as an electrode. In short, 20 mg of catalyst and 50 μL of Nafion solution were dispersed in ethanol (1.5 ml) and H_2O (1.5 ml) mixed solution under ultrasonication for 1 h to obtain a homogeneous catalyst ink. Afterwards, 20 μL of as-prepared ink was drop-cast onto commercial Ni foam with 0.16 cm^2, and then repeat the drop-casting process 3 times. CV scans were recorded at

a scan rate of 1 mV s^{-1}. The OER chronoamperometric measurement of CoFe LDH-*S* on commercial Ni foam was performed at overpotential of 250 mV.

3) Carbon cloth

To gather XPS spectra, Raman spectra and XRD patterns of post-catalyst, the dense and electro-conductive carbon cloth was used as electrodes. The fresh prepared CoFe LDH-*S* without drying was re-dispersed in water to form concrete-like slurry. Afterwards, the red slurry was homogeneously painted on the carbon cloth and dried slowly in air at room temperature the (Fig. S13b), assuring a good cohesiveness between carbon cloth and catalyst. The OER chronoamperometric measurement of CoFe LDH-*S* on carbon cloth was carefully performed at 1.5 V vs. RHE in home-made electrochemical cells, keeping the red side of carbon cloth upturned to avoid the detachment of catalyst. Finally, the black post-catalyst was discreetly rinsed in deionized water and dried in room temperature.

Turnover frequency (TOF) calculation

To estimate the TOFs of Co-Fe LDHs for OER, the following equation was used,[4]

$$TOF = J \cdot A/4F \cdot n$$

where J is the current density at a given overpotential (η = 300 mV), A is the surface area of the electrode, F is Faraday constant (96485.3 C mol^{-1}) and m is the mole of active sites in deposited catalyst on GC electrode. All the metal cations were regarded as active sites for OER in this case.

Physical characterization

X-ray diffraction (XRD) patterns were collected on Bruker D8 Advance diffractometer with Cu Kα radiation (λ = 1.54056 Å). Transmission electron microscope (TEM) was performed on a JEOL JEM 2100F for the gaining of Co hydroxide and CoFe hydroxides microstructures. X-ray photoelectron spectroscopy (XPS) was collected on a Thermo Scientific Escalab 250Xi, using C 1s (284.8 eV) for calibration. Raman spectra were conducted on a Raman microspectrometer (Horiba HR-800) with excitation laser wavelength at 633 nm. The surface morphologies were

detected via tapping mode AFM on silicon wafer. Inductively coupled plasma mass spectrometry (ICP-MS) was conducted on Thermo Scientific Ultimate 3000+iCAP RQ for the detection of dissolved Fe and Co species in KOH electrolyte after long-term stability measurement. Prior to the ICP-MS measurement, the residual electrolyte was diluted and acidized by nitric acid. X-ray absorption spectra (XAS) including X-ray absorption near-edge structure (XANES) and extended X-ray absorption fine structure (EXAFS) of the samples at Fe K-edge and Ni K-edge were both collected at the Singapore Synchrotron Light Source (SSLS) center, where a pair of channel-cut Si (111) crystals was used in the monochromator. The Fe and Ni K-edge XANES data were recorded in a transmission mode. The storage ring was working at the energy of 2.5 GeV with an average electron current of below 200 mA. The acquired EXAFS data were extracted and processed according to the standard procedures using the ATHENA module implemented in the IFEFFIT software packages.

Computational details

We have employed the Vienna Ab initio Simulation Package (VASP) to perform all density functional theory (DFT) calculations within the generalized gradient approximation (GGA) using the Perdew-Burke-Ernzerhof (PBE) functional. We have chosen the projected augmented wave (PAW) potentials to describe the ionic cores and taken valence electrons into account using a plane wave basis set with a kinetic energy cutoff of 450 eV. Geometry optimizations were performed with the force convergency smaller than 0.05 eV/Å. The DFT-D3 empirical correction method was employed to describe van der Waals interactions. U-values, which are applied to d-orbitals of Fe and Co are taken as 2.56 and 3.50 eV, respectively. Monkhorst-Pack k-points of 2×5×1 were applied for all the calculation. All the atoms are relaxed in all the calculations. Free energy corrections were conducted in this work at the temperature of 300 K.

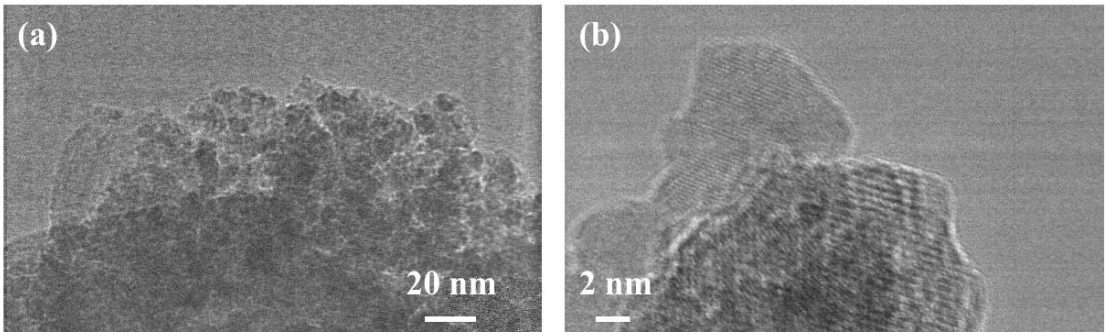

Fig. S1 TEM images of CoFe LDH-*Bulk*.

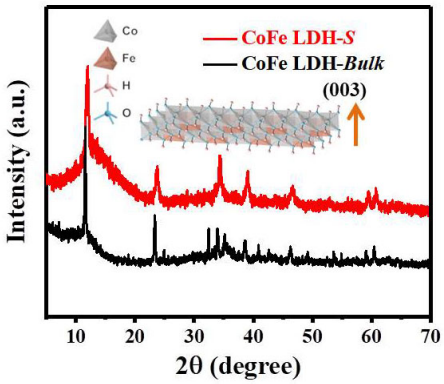

Fig. S2 XRD patterns of CoFe LDH-*S* and CoFe LDH-*Bulk*.

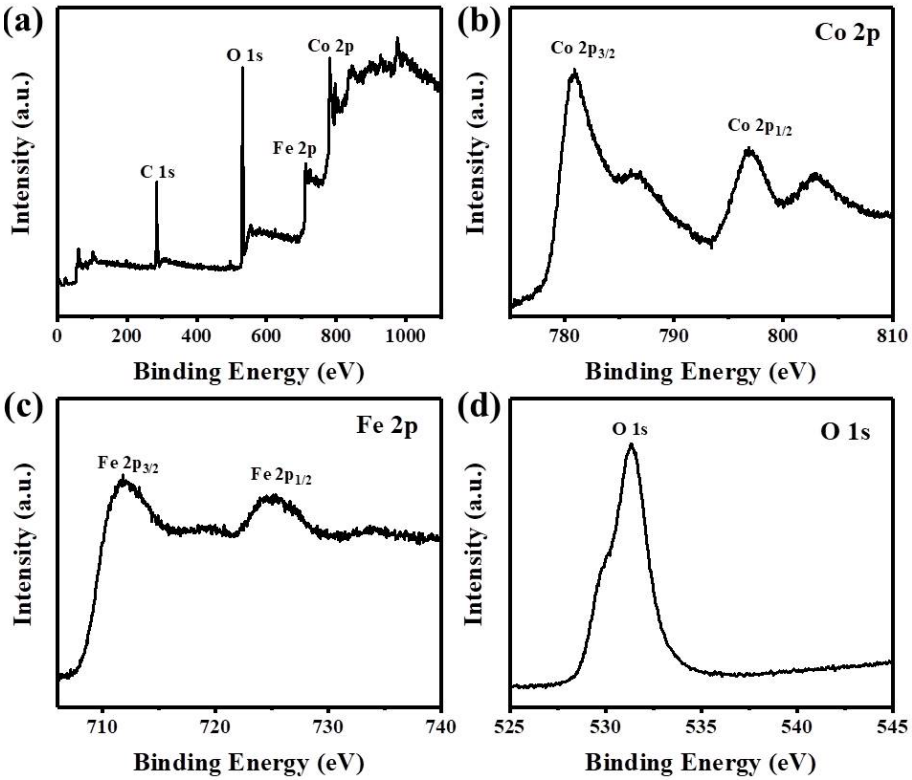

Fig. S3 (a) XPS survey spectra of CoFe LDH-*S* and high-resolution XPS spectra for (b) Co 2p, (c) Fe 2p and (d) O 1s of Co-Fe LDH-*S*.

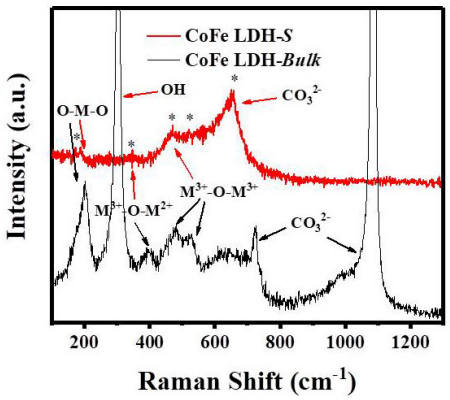

Fig. S4 Raman spectra of CoFe LDH-*S* and CoFe LDH-*Bulk*.

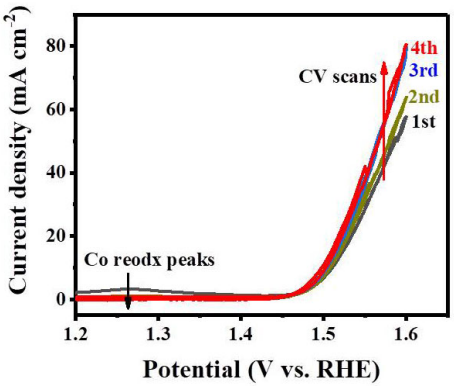

Fig. S5 CV curves of Co-Fe LDH-*S*, measured in 1.0 M KOH electrolyte at a scan rate of 5 mV s^{-1}.

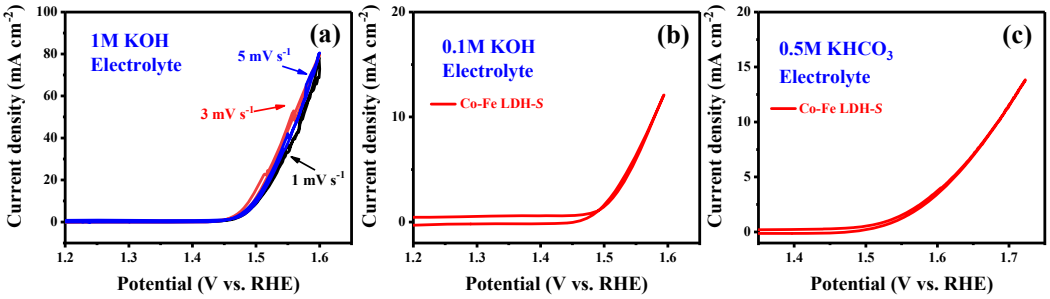

Fig. S6 (a) CV curves of Co-Fe LDH-*S*, measured in 1.0 M KOH electrolyte at a scan rate of 1 mV s^{-1}, 3 mV s^{-1} and 5 mV s^{-1}. CV curves of Co-Fe LDH-*S*, measured in (b) 0.1 M KOH and (c) 0.5 M $KHCO_3$ (pH = 7.2) at a scan rate of 5 mV s^{-1} , respectively.

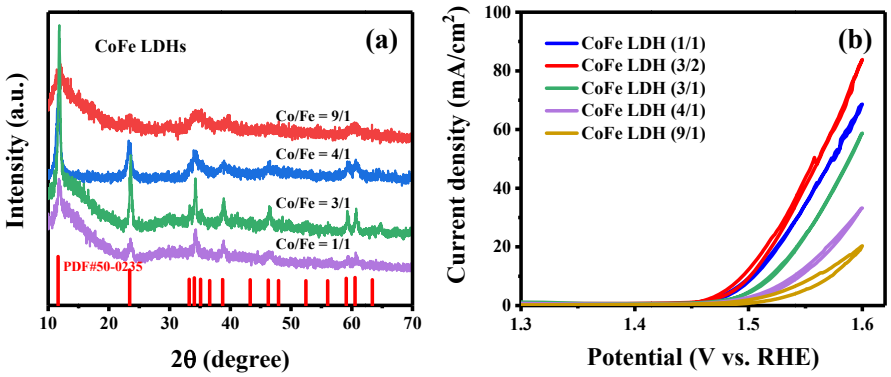

Fig. S7 XRD patterns of CoFe LDHs and the standard PDF cards of CoFe LDH. CV curves of CoFe LDHs with varied atomic ratio of Co/Fe, measured in 1 M KOH electrolyte at a scan rate of 5 mV s^{-1}.

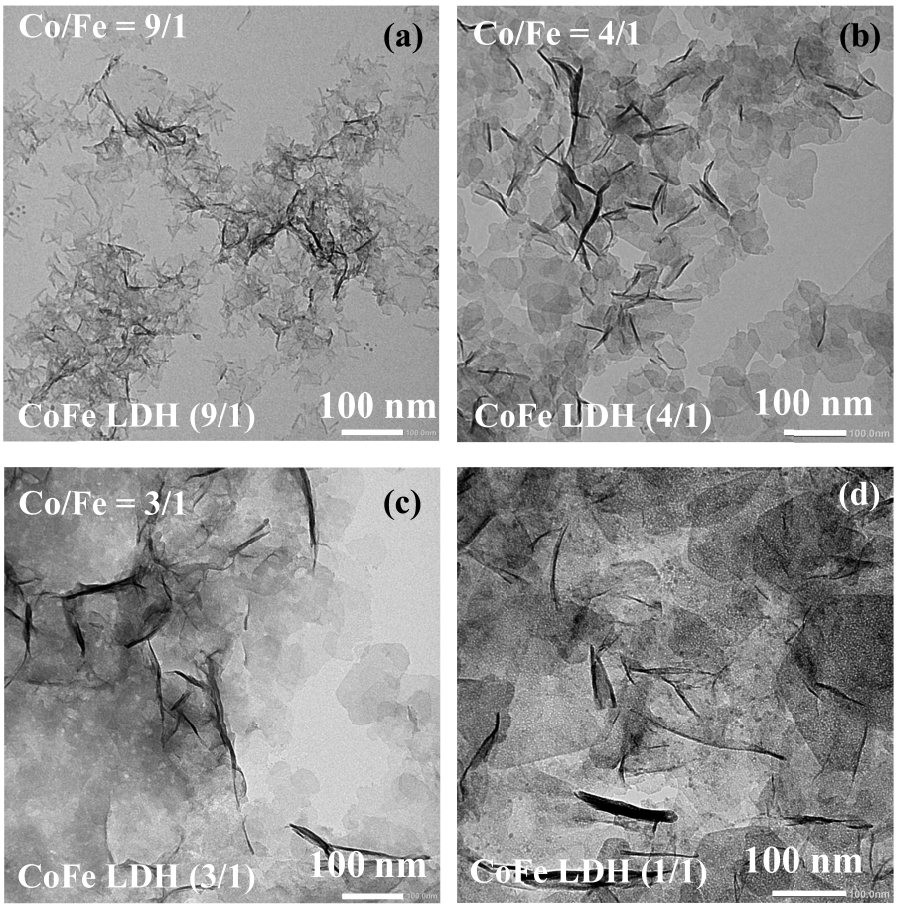

Fig. S8 TEM images of CoFe LDH (9/1), CoFe LDH (4/1), CoFe LDH (3/1) and CoFe LDH (1/1).

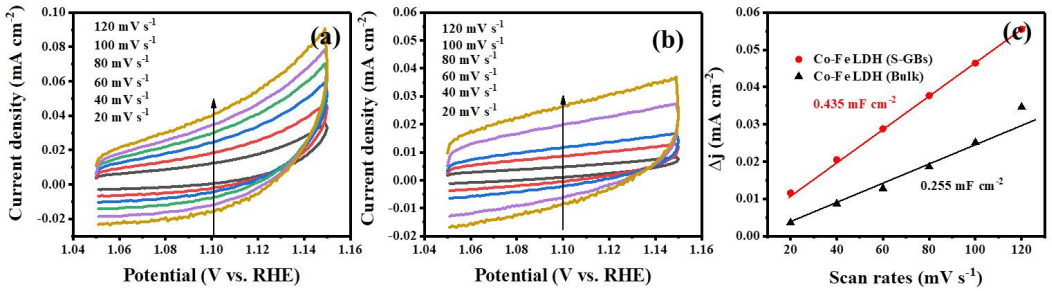

Fig. S9 CVs of (a) CoFe LDH-*S* and (b) CoFe LDH-*Bulk* from 1.05 V to 1.15 V vs. RHE. (c) Determination of C_{dl} of the two samples.

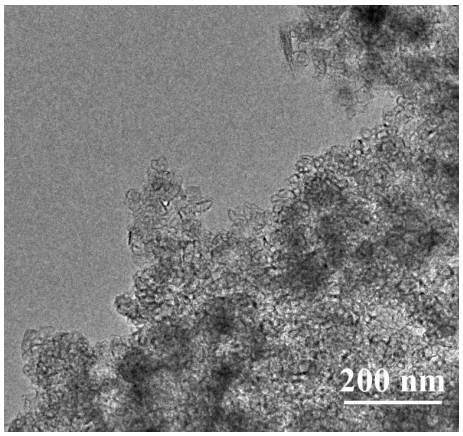

Fig. S10 TEM image of CoFe LDH-*S* after a long-term OER stability test.

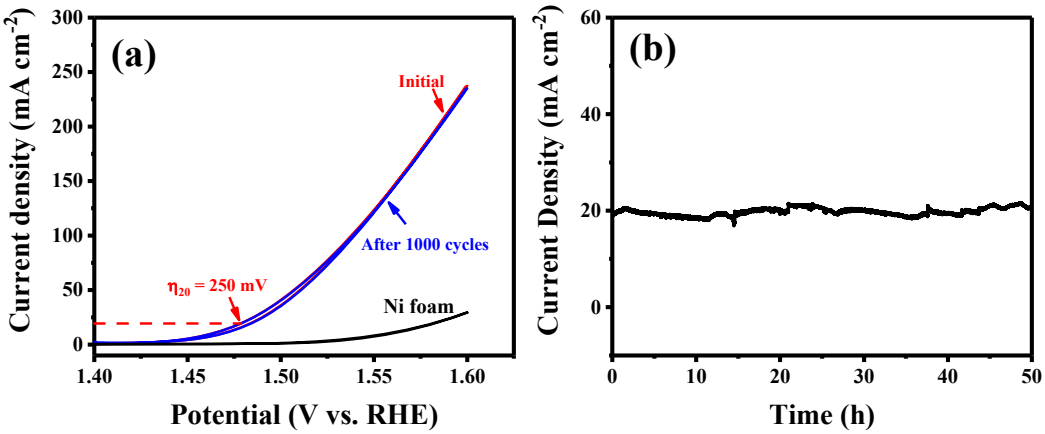

Fig. S11 (a) CV curves of Co-Fe LDH-*S* on Ni foam before and after 1000 cycles, measured in 1.0 M KOH electrolyte at a scan rate of 1 mV s^{-1}. (b) OER chronoamperometric measurement of CoFe LDH-*S* on Ni foam at η = 250 mV.

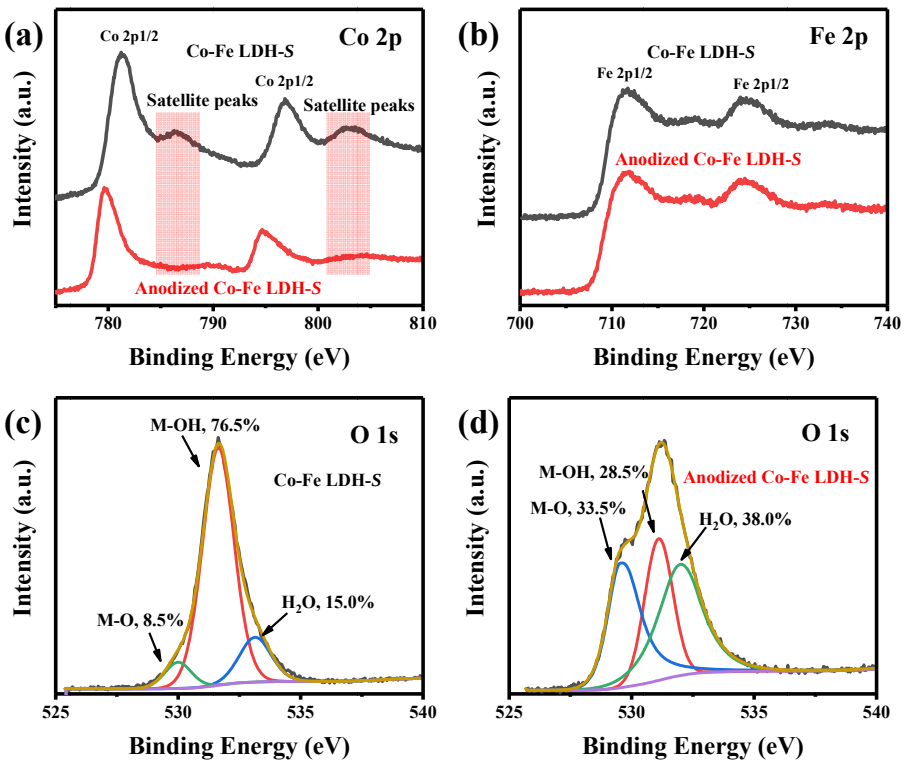

Fig. S12 High-resolution XPS spectra for (a) Co 2p and (b) Fe 2p of Co-Fe LDH-*S* and anodized Co-Fe LDH-*S*. High-resolution XPS spectra for O 1s of (c) Co-Fe LDH-*S* and (d) anodized Co-Fe LDH-*S*. The dark curve of Co-Fe LDH-*S* and anodized Co-Fe LDH-*S* are the experimental results. The yellow curves are the summation of the three synthetic peaks (green, red and blue curves). All the spectra are corrected by the C 1s peak of 284.8 eV.

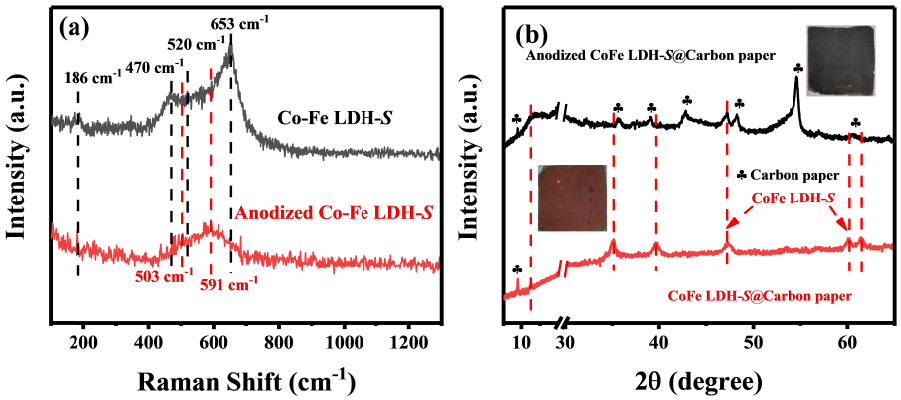

Fig. S13 (a) Raman spectra and (b) XRD patterns of Co-Fe LDH-*S* and anodized Co-Fe LDH-*S*.

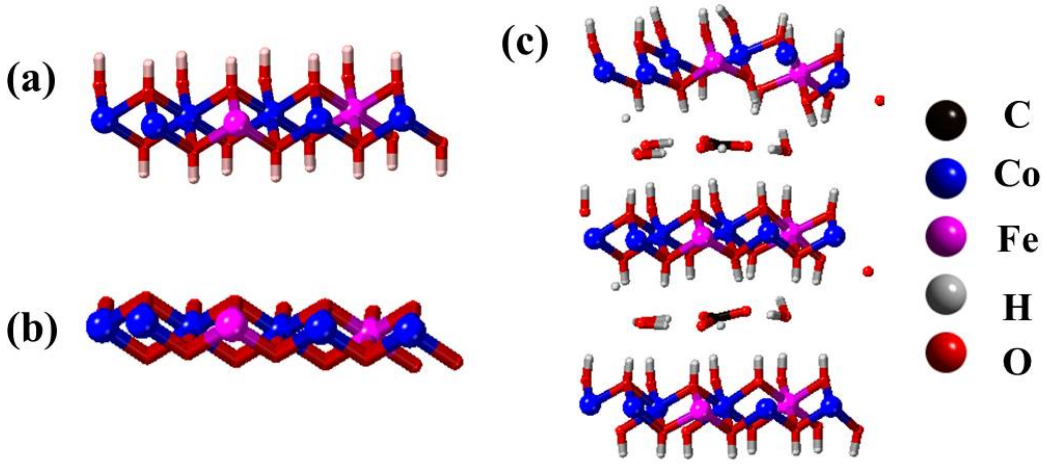

Fig. S14 Simulated crystal structures of (a) α-CoFe LDH-*S*, (b) CoFe LDH-*S* and (c) α-CoFe LDH-*Bulk*.

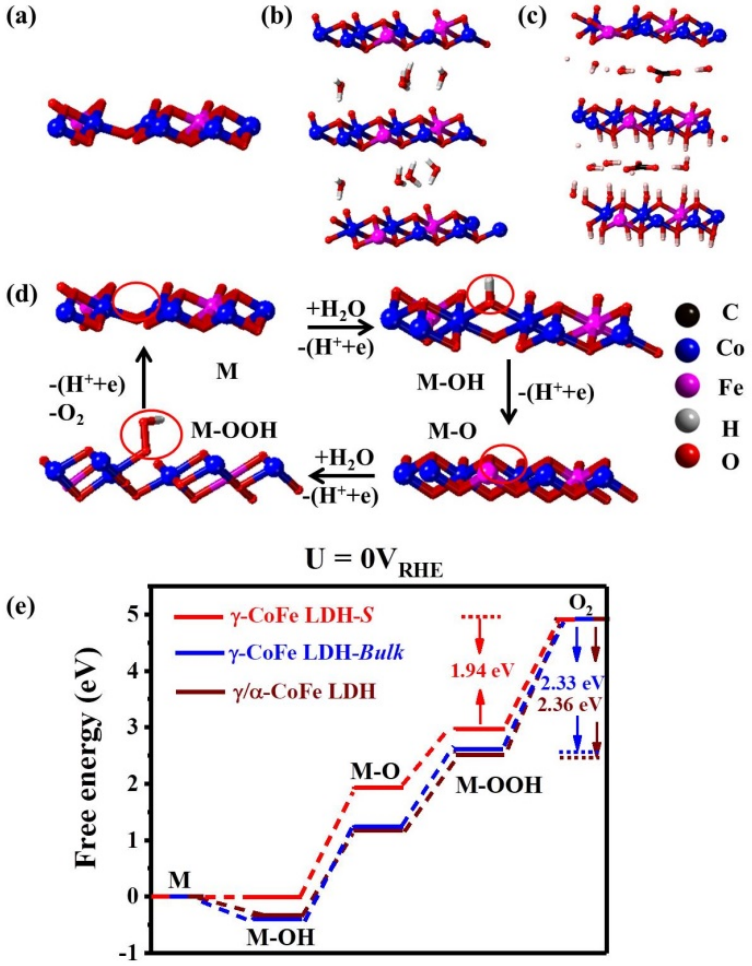

Fig. S15 Simulated crystal structures of (a) γ-CoFe LDH-*S*, (b) γ-CoFe LDH-*Bulk* and (c) γ/α-CoFe LDH with oxygen vacancies. (d) Proposed OER pathway on γ-CoFe. (f) Reaction free-energy diagrams for OER on γ-CoFe LDH-*S*, γ-CoFe LDH-*Bulk* and γ/α-CoFe LDH.

Table S1. Reaction free-energy diagrams for OER on γ-CoFe LDH-*S*, γ-CoFe LDH-*Bulk* and γ/α-CoFe LDH.

	M → MOH	MOH → MO	MO → MOOH	MOOH → O_2
γ-CoFe LDH-*S*	0.001 eV	1.92 eV	1.05 eV	1.95 eV
γ-CoFe LDH-*Bulk*	-0.39 eV	1.63 eV	1.34 eV	2.33 eV
γ/α-CoFe LDH	-0.33 eV	1.51 eV	1.38 eV	2.36 eV

The highest reaction free energy barriers (ΔG) are marked in red.

Supplementary Note 1

The M-O peak shift and the greatly reduced peak in the EXAFS spectra intensity in the second shell.

The M-O peak shift and the greatly reduced peak in the EXAFS spectra intensity in the second shell are caused by crystal vacancies, especially cation defect in this case. The amplitude of R space depends on the coordination number and mean-square disorder, with positive correlation with a high coordination number and negative correlation with a low meansquare disorder, and vice versa.[5, 6] Therefore, the greatly reduced peak in the second shell indicates the CoFe LDH-*S* enriches more cation defect (e.g. Co, Fe) compared to that of Co-Fe LDH- *Bulk*. This is in consistence with the cases of Co_3O_4, $Ni(OH)_2$ and NiO with cation vacancies which lead to a greatly reduced peak in the EXAFS spectra intensity in the second shell.[5, 7, 8] Meanwhile, the crystal vacancies also give rise to altering the average distance of neighboring M atoms with O atoms, leading to the M-O peak shift.

Supplementary Note 2

The dynamic stability of CoFe LDH-*S*

The concentrations of dissolved Fe and Co species in 1.0 KOH detected by ICP are 0.84 and 0.12 ppm, respectively. Traditionally, Fe species in electrocatalyst are relatively unstable under intense oxidizing condition in comparison to that of Co species and loss as FeO_4^{2-} species, giving rise to a decreased OER performance.[9, 10]

However, the dissolved FeO_4^{2-} species can be re-deposited over a CoO_xH_y host in 1.0 M KOH, leading to a trace amount of FeO_4^{2-} species in electrolyte and therefore retaining a stable water oxidation activity.[11]

Supplementary Note 3
The real electrocatalyst during the water oxidation

XPS, Raman and XRD investigations were supplemented to characterize the spent catalysts, which identified that the CoFe LDH-*S* transforms into $Co_xFe_{1-x}OOH$ species. The Co 2p XPS profiles of anodized CoFe LDH-*S* moves toward lower binding energy in contrast to the pristine one, while Fe 2p almost remains unchanged (Fig. S12a and S12b). Meanwhile, the satellite peak of Co 2p almost disappears which are associated with the bivalent cobalt species. Meanwhile, the signal assigned to the M-O of oxyhydroxides significantly increases (Fig. S12c and S12d), indicating the generation of Co^{3+} species (e.g., γ-CoOOH).[12, 13] These both indicate the oxidation of Co^{2+} into Co^{3+} species under polarization conditions. Moreover, Raman spectra provide consistent evidences (Fig. S13a). The new vibration at 503 and 591 cm^{-1} are assigned to CoOOH,[14, 15] but the peaks associated with brucite-like LDH become weak. This in line with the weakened diffraction peaks of LHD after OER test in XRD patterns (Fig. S13b). The reddish brown CoFe LDH-*S* also transforms into black $Co_xFe_{1-x}OOH$ species (Inset of Fig. S13b).

References：

1. Y. Wang, C. Xie, Z. Zhang, D. Liu, R. Chen and S. Wang, *Adv. Funct. Mater.*, 2018, **28**, 1703363.
2. Y. Zhou, W. Zhang, J. Hu, D. Li, X. Yin and Q. Gao, *ACS Sustainable Chem. Eng.*, 2021, **9**, 7390-7399.
3. F. Dionigi and P. Strasser, *Adv. Energy Mater.* , 2016, **6**, 1600621.
4. T. Bhowmik, M. K. Kundu and S. Barman, *ACS Appl. Energy Mater.*, 2018, **1**, 1200-1209.
5. R. Zhang, Y.-C. Zhang, L. Pan, G.-Q. Shen, N. Mahmood, Y.-H. Ma, Y. Shi, W. Jia, L. Wang, X. Zhang, W. Xu and J.-J. Zou, *ACS Catal.*, 2018, **8**, 3803-3811.
6. Z. Sun, W. Yan, T. Yao, Q. Liu, Y. Xie and S. Wei, *Dalton Trans.*, 2013, **42**, 13779-13801.

7. Q. He, Y. Wan, H. Jiang, Z. Pan, C. Wu, M. Wang, X. Wu, B. Ye, P. M. Ajayan and L. Song, *ACS Energy Lett.* , 2018, **3**, 1373-1380.

8. Y. Zhao, X. Jia, G. Chen, L. Shang, G. I. Waterhouse, L. Z. Wu, C. H. Tung, D. O'Hare and T. Zhang, *J. Am. Chem. Soc.*, 2016, **138**, 6517-6524.

9. S. Zou, M. S. Burke, M. G. Kast, J. Fan, N. Danilovic and S. W. Boettcher, *Chem. Mater.*, 2015, **27**, 8011-8020.

10. K. Obata and K. Takanabe, *Angew Chem. Int. Ed.* , 2018, **57**, 1616-1620.

11. D. Y. Chung, P. P. Lopes, P. Farinazzo Bergamo Dias Martins, H. He, T. Kawaguchi, P. Zapol, H. You, D. Tripkovic, D. Strmcnik, Y. Zhu, S. Seifert, S. Lee, V. R. Stamenkovic and N. M. Markovic, *Nat. Energy*, 2020, **5**, 222-230.

12. J. Yang, H. Liu, W. N. Martens and R. L. Frost, *J. Phys. Chem. C*, 2010, **114**, 111–119.

13. T. Xue and J.-M. Lee, *J. Power Sources*, 2014, **245**, 194-202.

14. T. Pauporte´, L. Mendoza, M. Cassir, M. C. Bernard and J. Chivotc, *J. Electrochem. Soc.*, 2005, **152**, C49-C53.

15. Y.-C. Liu, J. A. Koza and J. A. Switzer, *Electrochimica Acta*, 2014, **140**, 359-365.